INSTITUTE OF PHYSICS PUBLISHING MODELLING AND SIMULATION IN MATERIALS SCIENCE AND ENGINEERING

Modelling Simul. Mater. Sci. Eng. **9** (2001) 499–511 PII: S0965-0393(01)28716-6

Morphological evolution during phase separation and coarsening with strong inhomogeneous elasticity

Jingzhi Zhu[1], **Long-Qing Chen**[1] **and Jie Shen**[2]

[1] Department of Materials Science and Engineering, Penn State University, University Park, PA 16802, USA
[2] Department of Mathematics, Penn State University, University Park, PA 16802, USA

Received 7 May 2001, accepted for publication 28 August 2001
Published 8 October 2001
Online at stacks.iop.org/MSMSE/9/499

Abstract

We studied the morphological evolution during spinodal phase separation and subsequent coarsening in systems with a strong dependence of elastic constants on the composition. An efficient numerical method is developed for solving the two-dimensional inhomogeneous elastic equilibrium equations by using the conjugate gradient method. A simple model binary system with a symmetric miscibility gap is considered. It is shown that the early stages of spinodal phase separation in a solid solution with a 50–50% composition always result in an interconnected morphology, regardless of the degree of elastic inhomogeneity. For systems with strong elastic inhomogeneity, particle splitting and coalescence take place concurrently during coarsening. In the late stages, the morphology has the characteristics that the hard phase forms precipitates surrounded by the soft phase which forms the matrix, similar to that predicted previously by others using first-order approximations. An analysis of the coarsening kinetics shows that although the growth exponent decreases with the increase in the degree of elastic inhomogeneity, there is no freezing of the coarsening kinetics for all the cases that we studied, in contrast to that predicted previously by others. The effect of an externally applied strain on the two-phase morphology in the elastic regime is also discussed.

1. Introduction

Elastic strain energy is often generated during a solid-state phase transformation, and it plays a critical role in determining the transformation path and the corresponding microstructure evolution. Different theoretical approaches have been proposed for modelling the effects of elastic energy on coherent precipitate morphology and coarsening during precipitation reactions, including sharp-interface models, diffuse-interface models and discrete lattice models, see [1, 2] for reviews. For simplicity, most existing models make the homogeneous modulus approximation where the elastic moduli difference between different phases is

neglected. In this approximation, it was shown long ago by Khachaturyan that the total elastic energy for arbitrary coherent microstructure can be obtained in an analytical form in the Fourier space if the microstructure is macroscopically homogeneous [3, 4]. Khachaturyan's approach has been extensively used in computer simulations of coherent phase transformation and microstructure evolution using microscopic and continuum diffuse-interface field models [5–17]. The homogeneous approximation has also generally been assumed in the sharp-interface modelling of coherent precipitate morphologies and coarsening kinetics [18–23]. Many of the morphological transformations in coherent solids were satisfactorily explained even with the homogeneous approximation.

It has long been recognized that elastic modulus inhomogeneity can also significantly affect the coherent precipitate morphology. For example, it was shown by Eshelby that an ellipsoid precipitate has less elastic energy than a spherical one if the precipitate is less rigid than the matrix [24]. It was also noted by Johnson and Cahn that a softer domain in a harder matrix changes its shape as its size grows [25]. However, the elastic solutions become considerably more complicated for elastic inhomogeneous systems with arbitrary microstructures. Different modelling techniques have been proposed in recent years with which to study the microstructure evolution in elastically inhomogeneous systems. Schmidt and Gross [26] and Schmidt *et al* [27] have investigated the effect of elastic inhomogeneity on the equilibrium shape of a single particle as well as the interactions between two coherent particles, using a boundary integral formulation with a sharp-interface description. However, the temporal microstructure evolution through diffusional transport was not considered. Jou *et al* [28] also used the boundary integral method to calculate the diffusion and elastic fields in anisotropic and inhomogeneous systems by simultaneously solving the diffusion equation and elasticity equation. Since the precipitate–matrix interfaces are assumed to be sharp, it is difficult to handle certain morphological patterns which may occur during the initial stage of spinodal phase separation and during precipitate coalescence or splitting. Lee proposed a discrete atom method (DAM) which allowed rather arbitrary elastic inhomogeneity and precipitate morphologies [29, 30]. The effect of elastic energy on coherent precipitate morphology in elastically inhomogeneous systems has also been studied using the diffuse-interface approach by solving the elastic equilibrium equation using the zeroth- or first-order approximations [31–38]. It was shown by Onuki and Furukawa [38] that during spinodal decomposition and the subsequent coarsening in an elastically isotropic system where the shear modulus depends weakly on the local composition, the elastic misfit produces a percolated network of anisotropically deformed softer regions wrapping elastically isotropic harder domains and the coarsening rate is dramatically slowed down and even frozen. In a more recent attempt, Hu and Chen developed an iterative approach to solve the elasticity equation for systems with strong elastic inhomogeneity [39]. They showed that although prior calculations using first-order approximations predicted qualitatively the correct morphology in an elastically inhomogeneous two-phase system, the local stress distribution can be in serious error quantitatively if the modulus inhomogeneity is large.

The purpose of this paper is to describe a diffuse-interface approach for studying the coherent microstructural evolution in an elastically isotropic or anisotropic system with strong elastic inhomogeneity. This approach is significantly different from the iterative approach proposed by Hu and Chen [39]. Specifically, we propose to directly solve the inhomogeneous elasticity equation at any given time using the so-called conjugate gradient method (CGM) method, which provides higher accuracy than previous works using first-order or higher-order approximations. A similar approach has been proposed by Leo *et al* [40]. The focus of this work is on the influence of elastic inhomogeneity on the morphological evolution and the coarsening kinetics as compared to those predicted previously using first-order approximations.

The effects of an externally applied strain on the coarsening morphology in the elastic regime are also investigated.

2. Elastic energy calculation

2.1. Elasticity equation

The description of microstructures in a diffuse-interface model considers field variables which are functions of spatial coordinates. The simplest possible microstructure is an iso-structural two-phase system which can be described by only one field variable, the composition field, $c(\boldsymbol{r})$. Within the bulk of the two phases, the composition assumes the equilibrium values c_1, c_2, determined by the phase diagram. Across the interface from one phase to another, there is a gradual change in composition. We assume the coherent condition at the interface, i.e. the two lattice planes adjust to each other by elastic displacements of atoms from their regular positions.

Let us consider a two-phase microstructure with inhomogeneous elastic moduli. For a given composition distribution, we assume that the local elastic modulus tensor can be presented in terms of the composition field in a linear form,

$$\lambda_{ijkl}(\boldsymbol{r}) = \lambda^0_{ijkl} + \lambda^1_{ijkl}\delta c(\boldsymbol{r}) \tag{1}$$

where $\delta c(\boldsymbol{r}) = c(\boldsymbol{r}) - c_0$, c_0 is the average composition as the zero stress reference, and λ^0_{ijkl}, λ^1_{ijkl} are two constants. $\delta c(\boldsymbol{r})$ can describe the spatial configuration of any arbitrary two-phase mixture. Let λ_{ijkl} and λ^*_{ijkl} be the elastic modulus tensors of the matrix phase and second phase, respectively. Then, $\lambda^0_{ijkl} = \omega\lambda^*_{ijkl} + (1-\omega)\lambda_{ijkl}$ can be generally considered as an arithmetically average modulus and ω is the volume fraction of the second phase. λ^1_{ijkl} is a constant proportional to the elastic moduli difference between the two phases $\lambda^*_{ijkl} - \lambda_{ijkl}$.

In an inhomogeneous system, the stress-free lattice parameter depends on the local composition. We consider a cubic material where the composition dependence of the lattice parameter follows Vegard's law, i.e. the lattice parameter varies linearly with the composition,

$$a(\boldsymbol{r}) = a_0 + \frac{\mathrm{d}a}{\mathrm{d}c}\delta c(\boldsymbol{r}) \tag{2}$$

where $a(\boldsymbol{r})$ and a_0 are, respectively, the lattice parameters of the solid solution of the composition $c(\boldsymbol{r})$ and of the reference solution of the composition c_0, and $\mathrm{d}a/\mathrm{d}c$ is the derivative of the lattice parameter with respect to the local composition. The local stress-free strain $\epsilon^0_{kl}(\boldsymbol{r})$, which characterizes the lattice mismatch between the reference solution and a heterogeneity of the local composition $c(\boldsymbol{r})$, can be written as,

$$\epsilon^0_{kl}(\boldsymbol{r}) = \frac{a(\boldsymbol{r}) - a_0}{a_0} = \epsilon_0\delta c(\boldsymbol{r})\delta_{kl} \tag{3}$$

where $\epsilon_0 = (1/a_0)(\mathrm{d}a/\mathrm{d}c)$ is the composition expansion coefficient, and δ_{kl} is the Kronecker-delta function.

The total strain $\epsilon_{kl}(\boldsymbol{r})$ can be written as a sum of the homogeneous strain $\bar{\epsilon}_{kl}$, which determines the macroscopic shape and volume change produced by internal stress and externally applied stress, and an inhomogeneous local strain $\delta\epsilon_{kl}(\boldsymbol{r})$ defined by

$$\epsilon_{kl}(\boldsymbol{r}) = \bar{\epsilon}_{kl} + \delta\epsilon_{kl}(\boldsymbol{r}) \tag{4}$$

where the local strain $\delta\epsilon_{kl}(\boldsymbol{r})$ is related to the local displacement field $\boldsymbol{u}(\boldsymbol{r})$ by the usual elasticity relation,

$$\delta\epsilon_{kl} = \tfrac{1}{2}(u_{k,l} + u_{l,k}) \tag{5}$$

in which $u_{k,l}$ means $\partial u_k/\partial u_l$. The elastic strain is the difference between the total strain and the stress-free strain written as

$$\epsilon_{kl}^{\mathrm{el}}(\boldsymbol{r}) = \epsilon_{kl}(\boldsymbol{r}) - \epsilon_{kl}^{0}(\boldsymbol{r}). \tag{6}$$

The stress tensor $\sigma_{ij}(\boldsymbol{r})$ is related to the elastic strain tensor by Hooke's law according to the linear elasticity theory, i.e.

$$\begin{aligned}\sigma_{ij}(\boldsymbol{r}) &= \lambda_{ijkl}(\boldsymbol{r})\epsilon_{kl}^{\mathrm{el}}(\boldsymbol{r}) \\ &= [\lambda_{ijkl}^{0} + \lambda_{ijkl}^{1}\delta c(\boldsymbol{r})][\bar{\epsilon}_{kl} + \delta\epsilon_{kl}(\boldsymbol{r}) - \epsilon_{kl}^{0}(\boldsymbol{r})]\end{aligned} \tag{7}$$

where (1), (4) and (6) are used. The mechanical equilibrium condition requires that

$$\frac{\partial \sigma_{ij}}{\partial r_j} = 0. \tag{8}$$

Substituting (3), (5) and (7) into (8), we obtain

$$\frac{\partial}{\partial r_j}[\lambda_{ijkl}^{0} + \lambda_{ijkl}^{1}\delta c(\boldsymbol{r})]\frac{\partial u_k}{\partial r_l} = \frac{\partial \delta c(\boldsymbol{r})}{\partial r_j}[(2\lambda_{ijkl}^{1}\delta c(\boldsymbol{r}) + \lambda_{ijkl}^{0})\epsilon_0\delta_{kl} - \lambda_{ijkl}^{1}\bar{\epsilon}_{kl}]. \tag{9}$$

Equation (9) is the equilibrium equation of the elastic displacement fields that we need to solve in order to calculate the elastic energy. Periodic boundary conditions are applied for all dimensions in our study. All the partial derivatives in (9) can thus be conveniently calculated by using fast Fourier transforms (FFT). For given elastic constants λ_{ijkl}^{0}, λ_{ijkl}^{1}, homogeneous strain $\bar{\epsilon}_{kl}$, composition expansion coefficient ϵ_0 and composition distribution $\delta c(\boldsymbol{r})$ in the system, the right-hand side of (9) can be evaluated as a function of the spatial coordinates which we have denoted as $f_i(\boldsymbol{r})$.

2.2. Solution to the elasticity equation

The inhomogeneous elasticity, (9), can hardly be solved analytically due to its nonlinear nature. Therefore accurate and efficient numerical algorithms need to be developed. To simplify the mathematical problem, most existing methods have used either zeroth-order or first-order approximations of (9) where an inaccuracy in the numerical solutions may exist, especially for a strong inhomogeneous elasticity problem. Our aim is to solve (9) directly without making the first-order or higher-order approximations. We want to address the effects of elastic inhomogeneity by also considering the elastic anisotropy and an externally applied load. Similar to the approach by Leo *et al* [40], we propose to use the conjugate gradient method (CGM) which is effective for positive definite systems. It proceeds by generating vector sequences of iterates (i.e. successive approximations of the solution), residuals corresponding to the iterates, and search directions in updating the iterates and residuals [41]. The convergence rate of the conjugate gradient method depends on the condition number κ_{c} of the coefficient matrix. In fact, for a given tolerance, the conjugate gradient method converges in $O(\sqrt{\kappa_{\mathrm{c}}})$ iterations. In order to accelerate the convergence, it is a common practice to use a preconditioner.

A preconditioner is a matrix that can transform the underlying linear system into an equivalent one but with a smaller condition number. For example, let $\mathcal{L}$ be the operator on the elastic displacement field $\boldsymbol{u}$ in (9). Therefore (9) can be written in a simple form as $\mathcal{L}\boldsymbol{u} = \boldsymbol{f}$. If a preconditioning operator L approximates $\mathcal{L}$ in some way, then the transformed system

$$L^{-1}\mathcal{L}\boldsymbol{u} = L^{-1}\boldsymbol{f} \tag{10}$$

has the same solutions as the original system $\mathcal{L}\boldsymbol{u} = \boldsymbol{f}$, but we expect the condition number of $L^{-1}\mathcal{L}$ to be much smaller than that of $\mathcal{L}$, which can result in a faster convergence rate of the solutions.

We need to choose a preconditioner L that is a good approximation to $\mathcal{L}$ and also is easier to solve than $\mathcal{L}$. One good choice with which to approximate the operator $\mathcal{L}$ is to use the operator L defined by

$$Lu_i = \lambda^0_{ijkl}\frac{\partial^2 u_k}{\partial r_j \partial r_l}$$

where λ^0_{ijkl} is a constant representing a certain average of λ_{ijkl}. The operator L can be explicitly inverted in Fourier space with periodic boundary conditions. Indeed, by transforming u_k and δc into Fourier space, the approximate equation of (9)

$$Lu_i = \lambda^0_{ijkl}\frac{\partial^2 u_k}{\partial r_j \partial r_l} = \sigma^0_{ij}\frac{\partial \delta c(\boldsymbol{r})}{\partial r_j} \tag{11}$$

becomes, in Fourier space,

$$\lambda^0_{ijkl} g_j g_l u_k(\boldsymbol{g}) = -\mathrm{i}\sigma^0_{ij} g_j \delta c(\boldsymbol{g}) \tag{12}$$

where $\boldsymbol{g}$ is the wavevector in Fourier space, g_i is the ith component of $\boldsymbol{g}$, and $\sigma^0_{ij} = (2\lambda^1_{ijkl}\delta c(\boldsymbol{r}) + \lambda^0_{ijkl})\epsilon_0\delta_{kl} - \lambda^1_{ijkl}\bar{\epsilon}_{kl}$. For non-zero $\boldsymbol{g}$, the solution of the displacement $u_i(\boldsymbol{g})$ in Fourier space is

$$u_i(\boldsymbol{g}) = -\mathrm{i}G_{ij}(\boldsymbol{g})\sigma^0_{jk} g_k \delta c(\boldsymbol{g}) \tag{13}$$

where $(\boldsymbol{G}^{-1})_{ik}(\boldsymbol{g}) = \lambda^0_{ijkl} g_j g_l$. The corresponding displacements u_i in real space are then obtained by inverse Fourier transform.

With a constant-coefficient operator L as the preconditioner, we solve the inhomogeneous elasticity equation using the conjugate gradient method, which is implemented by the sparse linear algebra package (SLAP). The number of iterations for convergence needed for a given accuracy depends mainly on the ratio of the elastic constants between the two phases, and in a lesser context, on a number of other factors such as the stress-free strain, externally applied strain and the anisotropy of the material. In most cases, it takes two or three iterations to obtain a residual error of 10^{-7} if the elastic modulus difference between two phases is within the range of $\pm 100\%$. The larger the difference between the elastic constants between the two phases the greater the number of iterations needed. The proposed method can be applied to a system with good stability and accuracy where the elastic moduli between the phases can have a difference as large as a factor of ten, which is significantly higher than that allowed by the first-order or high-order approximations. A study of the convergence and accuracy of our preconditioned CGM and the iterative techniques for high-order approximations proposed by Hu and Chen is given in [39], where much higher accuracy is achieved in both the CGM method and iterative techniques than in the first-order approximation. Theoretically the proposed CGM method provides higher accuracy than any of the high-order approximations because the CGM method solves the inhomogeneous elastic equilibrium equation directly.

Once the elastic displacement fields u_i and the composition fields $c(\boldsymbol{r})$ are known, the elastic energy density can be calculated by

$$E_{\mathrm{el}} = \tfrac{1}{2}\sigma_{ij}\varepsilon^{\mathrm{el}}_{ij} = \tfrac{1}{2}\lambda_{ijkl}(\boldsymbol{r})\epsilon^{\mathrm{el}}_{ij}(\boldsymbol{r})\epsilon^{\mathrm{el}}_{kl}(\boldsymbol{r}) \tag{14}$$

where the elastic moduli $\lambda_{ijkl}(\boldsymbol{r})$ and the elastic strain tensor $\epsilon^{\mathrm{el}}_{ij}(\boldsymbol{r})$ are evaluated by (1) and (6), respectively.

3. Kinetic equations for microstructural evolution

In the phase-field modelling of phase separation and the subsequent coarsening in an isostructural two-phase system, the temporal evolution of a microstructure is determined by

solving the Cahn–Hilliard nonlinear diffusion equation [42],

$$\frac{\partial c}{\partial t} = M\nabla^2 \frac{\delta F}{\delta c} \tag{15}$$

where M is the mobility and F is the total free energy, which includes the bulk chemical free energy, the interfacial energy and the elastic strain energy. In the diffuse-interface model, the interfacial energy is introduced through the gradient energy terms. The total free energy in an inhomogeneous system is

$$F = \int_V [f(c) + E_{\mathrm{el}} + \tfrac{1}{2}\kappa(\nabla c)^2]\,\mathrm{d}V \tag{16}$$

where $f(c)$ is the local chemical free energy density, E_{el} is the elastic strain energy density, and κ is the gradient energy coefficient which can be related to interatomic interaction parameters. The variational derivative $\delta F/\delta c$ can thus be written as

$$\frac{\delta F}{\delta c} = \frac{\delta f}{\delta c} + \frac{\delta E_{\mathrm{el}}}{\delta c} - \kappa\nabla^2 c. \tag{17}$$

We choose the derivative $\delta f/\delta c$ with a form $\delta f/\delta c = 2(c-0.5)\left[-1+5(c-0.5)^2\right]$ which has two equilibrium composition values of approximately 0.053 and 0.947. $\delta E_{\mathrm{el}}/\delta c$ can be calculated without much difficulty by taking the variational derivative of the elastic energy density in (14) with respect to the composition field. Let us denote $g(c)$ as the term $\delta f/\delta c + \delta E_{\mathrm{el}}/\delta c$ in (17). For a given composition distribution, $g(c)$ can be computed explicitly after the elastic equilibrium equation is solved. The nonlinear temporal evolution equation for the composition field thus becomes

$$\frac{\partial c}{\partial t} = M\nabla^2[g(c) - \kappa\nabla^2 c]. \tag{18}$$

Recently we have developed a semi-implicit Fourier spectral method for solving the Cahn–Hilliard equation [43, 44]. Compared with the conventional forward Euler finite difference method, our method is orders of magnitude more efficient and accurate. The first-order semi-implicit Fourier spectral scheme for (18) is

$$(1 + \Delta t M\kappa k^4)\tilde{c}^{n+1}(\boldsymbol{k}) = \tilde{c}^n(\boldsymbol{k}) - \Delta t M k^2\{\tilde{g}(c^n)\}_{\boldsymbol{k}} \tag{19}$$

where $\boldsymbol{k} = (k_1, k_2)$ is a vector in the Fourier space, $k = \sqrt{k_1^2 + k_2^2}$ is the magnitude of $\boldsymbol{k}$, and $\tilde{c}(\boldsymbol{k})$ and $\{\tilde{g}(c)\}_{\boldsymbol{k}}$ represent the Fourier transform of $c(\boldsymbol{r})$ and $g(c)$, respectively. The details of this numerical approach can be found in [44].

At each time step, we solve the elastic equilibrium equation by the preconditioned conjugate gradient method for a given composition field $c(\boldsymbol{r})$. Then the evolution of the microstructure is obtained by updating the composition field using (19).

4. Results and discussion

Our simulations were performed on a square domain discretized using a lattice of 256×256 grid points with periodic boundary conditions. To illustrate the inhomogeneous elasticity effects, we select the average composition $c_0 = 0.5$ (the critical composition), which will result in equal volume fractions of the two phases in the equilibrium state as determined from the phase diagram. Initially the system is prepared in a homogeneous state by assigning a random number to each lattice site. The random numbers are uniformly distributed between 0.1 and -0.1 as the initial condition, corresponding to a high-temperature initial state where the composition deviation from the average value is only caused by fluctuation.

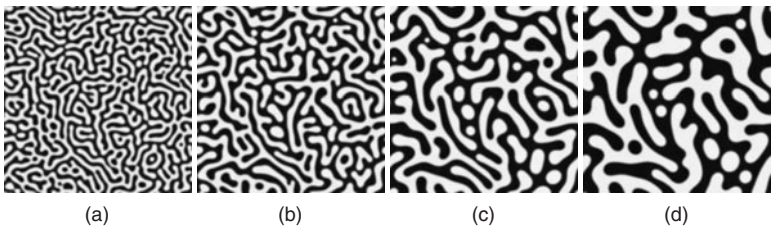

Figure 1. Morphological patterns of coarsening in an elastically isotropic and homogeneous system ($K_A = K_B$, $\mu_A = \mu_B$). (a) $t = 40$; (b) $t = 120$; (c) $t = 400$; (d) $t = 1000$.

To simplify the computation, most input parameters are scaled in dimensionless units. The typical parameters are: grid size $\Delta x = 1.0$, time step $\Delta t = 0.2$, gradient energy coefficient $\kappa = 1.0$, mobility $M = 1.0$, and the composition expansion coefficient $\varepsilon_0 = 0.07$. In comparison with the homogeneous elasticity equation (11), the inhomogeneous elasticity equation (9) takes more computation time in the conjugate gradient iterations. For a two-phase system where the elastic constants differ by 100% from each other, the total computation time is about three times that for an elastically homogeneous system.

In order to illustrate the effects of inhomogeneous elasticity on the morphological pattern evolution during phase separation and coarsening, we first studied a two-phase system with isotropic and homogeneous elasticity as the reference system. Figure 1 shows a typical example of its temporal evolution of morphological patterns during spinodal decomposition and subsequent coarsening. The grey levels represent the local compositions, with white representing high values and black representing low values. For the critical composition $c_0 = 0.5$, there is symmetry between the two phases forming interconnected domains. Shortly after the quench, there are well defined interfaces separating regions of different phases. The system evolves in such a way as to minimize the total free energy. Domain coarsening driven by the reduction of interfacial area is evident in figure 1.

We want to see how these morphologies are altered in an elastically isotropic but inhomogeneous system where the elastic constants of the two phases in equilibrium are different. A system with equal bulk modulus but with different shear modulus ratios (μ_A/μ_B) of the two phases is considered. In all of our later discussions, phase A always refers to the phase with higher equilibrium composition value and phase B refers to the one with lower equilibrium composition. An example of the microstructural evolution at four different times is shown in figure 2 where $\mu_A = 3\mu_B$. As can be seen from figure 2, the microstructure no longer has symmetry as in an interconnected morphology, but forms a pattern where particles of phase A with higher shear modulus are surrounded by phase B as the matrix with lower shear modulus, especially in the later stages. If, on the contrary, μ_A is less than μ_B, the morphology will be reversed where phase B forms isolated domains and phase A forms the matrix. These morphologies generally agree with those from Onuki and Furukawa [38] in that an elastically softer phase forms a percolated network and wraps the particles of the harder phase. The coarsening microstructures strongly depend upon the interplay between the interfacial and elastic energies. A minimization of the free energy requires that the elastically hard phase deforms less than the soft phase. The elastic energy is less for hard precipitates in a soft matrix than for soft precipitates in a hard matrix. Thus the morphology formed is such that most of the elastic energy is stored in the matrix which is made up of the more deformable, elastically softer phase wrapping the harder particles. The volume fraction of each phase is approximately 50% in our simulations. Nishimori and Onuki found that the soft phase could form the matrix even at a relatively small volume fraction [45].

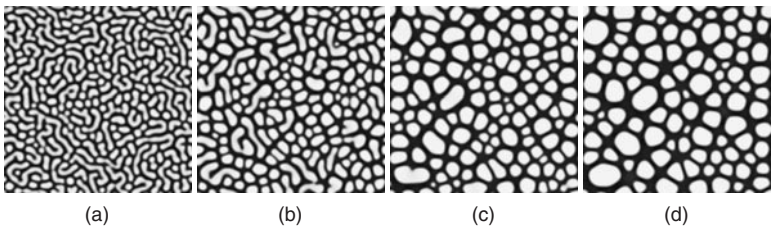

Figure 2. Morphological patterns of coarsening in an elastically isotropic and inhomogeneous system ($K_A = K_B$, $\mu_A = 3\mu_B$). (a) $t = 40$; (b) $t = 120$; (c) $t = 400$; (d) $t = 1000$.

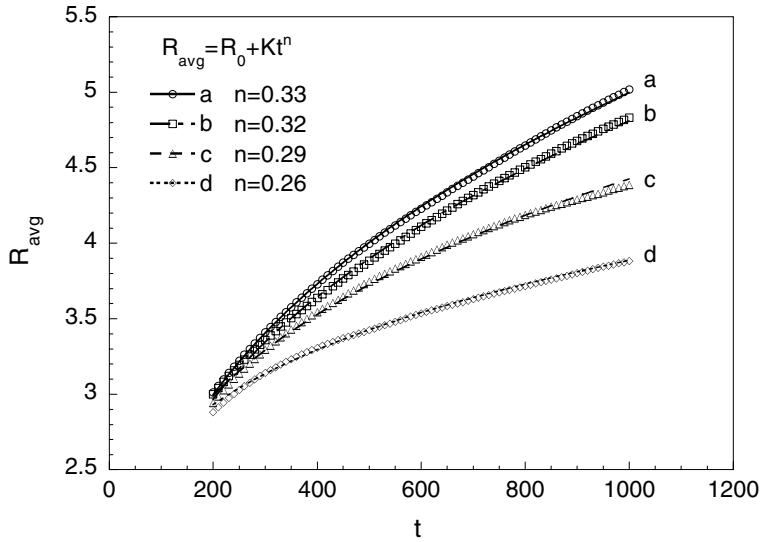

Figure 3. The average domain size R_{avg} as a function of time t for elastically isotropic and inhomogeneous systems with different shear moduli. (a) $\mu_A = \mu_B$; (b) $\mu_A = 1.3\mu_B$; (c) $\mu_A = 2\mu_B$; (d) $\mu_A = 3\mu_B$.

Elastic inhomogeneity can also affect the coarsening kinetics when interfacial energy becomes less important as the domain grows. A slowing down in coarsening may be expected for alloys where the shear moduli in the matrix and precipitates are different. In figure 3 we compare the measured average domain size R_{avg} (plotted by the open symbols) as a function of time t at a relatively late stage of coarsening for isotropic and inhomogeneous systems with different shear moduli ratios of the two phases. The average domain size is characterized by the inverse of the first moment of the structure function as a function of the wavenumber [44]. As the coarsening continues, the typical length scale increases for all systems. Curves a, b, c, and d represent the systems where $\mu_A/\mu_B = 1$, 1.3, 2 and 3, respectively. The higher the two phase shear moduli ratio, the lower the typical domain size at the same coarsening time. It was claimed by Onuki and Furukawa that domain growth could be frozen in cubic solids with elastic misfit [38]. We have not observed domain freezing in the above simulations. However, the coarsening does slow down due to the increase of elastic inhomogeneity.

It is usually observed that during the late stages of coarsening, two phase microstructures exhibit dynamical scaling (or self-similarity). When the scaling regime is reached, the average scale R_{avg} of the microstructure grows as a power law in time which can be written as

$$R_{\text{avg}} = R_0 + Kt^n \tag{20}$$

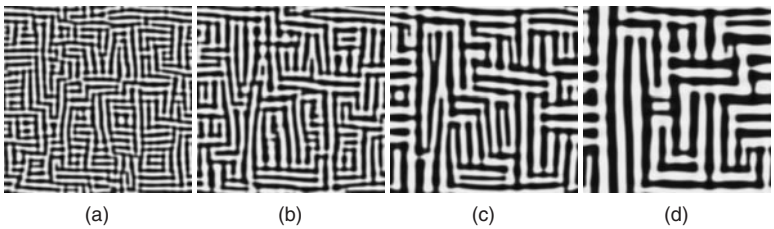

Figure 4. Morphological patterns of coarsening in an elastically anisotropic and homogeneous system ($C_{ij}^A = C_{ij}^B$). (a) $t = 40$; (b) $t = 100$; (c) $t = 400$; (d) $t = 1000$.

where K is called the coarsening rate, R_0 is the initial length scale and n is the growth exponent. In figure 3, a nonlinear fit in the form of (20) with different parameters of R_0, K and n is shown by curves of different line types. Curve a is plotted for coarsening in an elastically homogeneous system where $\mu_A = \mu_B$. The fitted growth exponent n for curve a is approximately 0.33, which is in good agreement with that in the LSW growth [46]. The coarsening rate constant K is about 0.5 for curve a. According to our analysis results, the addition of elastic inhomogeneity to the system only changes K by a small degree ($\pm 5\%$). However, the growth exponent n depends strongly on μ_A/μ_B. The corresponding values of n for curves b, c and d are 0.32, 0.29 and 0.26, respectively. Therefore the growth exponent decreases with increasing elastic inhomogeneity. The smaller the growth exponent is, the slower the coarsening occurs.

We also investigated the morphological evolution of an elastically anisotropic and homogeneous system. It was observed that an anisotropic system often develops strong spatial correlations along elastically soft crystallographic directions during coarsening even though the initial spatial configurations are nearly random. As coarsening continues, the matrix aligns itself and reshapes the domains to reduce the elastic energy. We consider a cubic system with a negative anisotropy $\xi_a \equiv (C_{11} - C_{12} - 2C_{44})/C_{44}$ of -1. In figure 4 we display the time evolution of the morphologies for a system where the two phases have equal elastic constants. The elastic soft directions are [10] and [01] if no external stress is applied. Domains are interconnected rectangular stripes aligned in the soft directions. The characteristic microstructural features were obtained by Nishimori and Onuki using a first-order approximation [32].

Figure 5 shows the microstructural patterns for an elastically anisotropic and inhomogeneous system. The two phases have the same elastic anisotropy as in figure 4. The elastic constants of phase A (displayed in white) are greater than those of phase B. Instead of forming interconnected stripes, the hard phase A forms many rectangular precipitates surrounded by the soft phase at $t = 400$ and 1000. The hard precipitates align themselves along the elastically soft directions [01] and [10] as shown in figure 4. If the system has a positive anisotropy, the precipitates will then align along the [11] direction. Considering the effect of elastic inhomogeneity on the morphology, a very important characteristic is that the hard phase always forms the precipitate while the soft phase always forms the matrix, as demonstrated clearly in both elastically isotropic and anisotropic systems. We simply define a parameter $\theta = (C_{ij}^A - C_{ij}^B)/C_{ij}^A$ to represent this elastic inhomogeneity in an anisotropic system. In figure 5 where θ is about 30%, many hard precipitates are rectangular with a large aspect ratio of the two sides in the early stages, as shown in figures 5(a) and 5(b). Accompanying the microstructure coarsening, the coalescence and splitting of precipitates are also evident. Two neighbouring hard precipitates will merge to form one large particle with the soft phase thin-wall between them disappearing. As coarsening continues, it is also observed that a particle with a rectangular stripe shape can possibly split into two particles with a smaller aspect

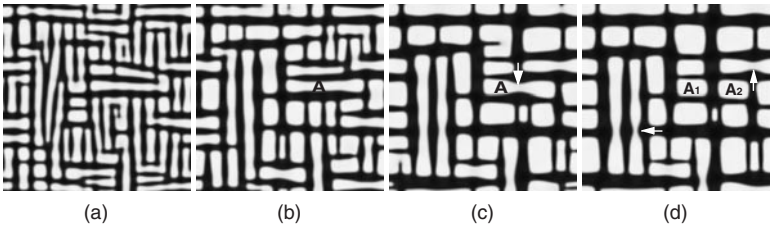

Figure 5. Morphological patterns of coarsening in an elastically anisotropic and inhomogeneous system ($C_{ij}^{A} = 1.3C_{ij}^{B}$). (a) $t = 400$; (b) $t = 1000$; (c) $t = 3000$; (d) $t = 4000$.

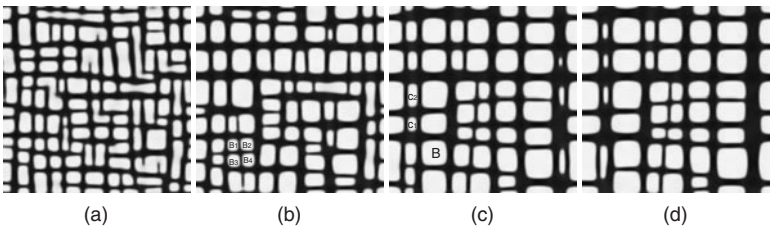

Figure 6. Morphological patterns of coarsening in an elastically anisotropic and inhomogeneous system ($C_{ij}^{A} = 2C_{ij}^{B}$). (a) $t = 400$; (b) $t = 1000$; (c) $t = 3000$; (d) $t = 4000$.

ratio. For example, precipitate A in figure 5(b) eventually splits into A_1 and A_2 as shown in figure 5(d). Necks are often formed in the middle of the long stripe during the splitting as shown by the arrows. The occurrence of particle splitting can be understood in terms of the competition between the elastic strain energy and the interfacial energy. The decrease in the elastic energy resulting from the splitting compensates for the increase in the interfacial energy. The particles are more square in form in the later stages than in the early stages of coarsening. A similar particle splitting phenomenon has been observed by Lee using DAM [30].

The morphology evolutions in a system with a larger elastic inhomogeneity $\theta = 100\%$ are shown in figure 6. Compared with the corresponding patterns for a system with a smaller elastic inhomogeneity shown in figure 5, the large inhomogeneity seems to produce more square-like precipitates for the same evolution time. In the early stage, microstructure coarsening by particle coalescence seems to be dominant, see for example, the merging of particles B_1, B_2, B_3 and B_4 in figure 6(b) to form particle B in figure 6(c). At a late stage of coarsening, the system average length scale increases resulting mainly from the dissolution of small domains with high interfacial curvature and the growth of neighbouring large domains with low curvature. For example, particles C_1 and C_2 in figure 6(c) later disappear and shrink, respectively, at $t = 4000$. Comparing the microstructure at $t = 3000$ (figure 6(c)) with that at $t = 4000$ (figure 6(d)), we can see that the coarsening dramatically slows down in the later stage due to the large elastic inhomogeneity, although freezing of the domains is not observed in our simulations.

The microstructural features of an alloy system can be influenced by an applied stress. Here we present our numerical simulations on phase separation and the subsequent coarsening constrained by applying a constant uniaxial strain in the elastic regime where interfacial dislocations and matrix plasticity are neglected. The total homogeneous strain is the applied strain which determines the macroscopic deformation of the system. From (9), we can predict that in an homogeneous elasticity system where the difference between the elastic constants of the two phases is zero, i.e. $\lambda_{ijkl}^{1} = 0$, the externally applied strain $\bar{\epsilon}_{kl}$ will not show any

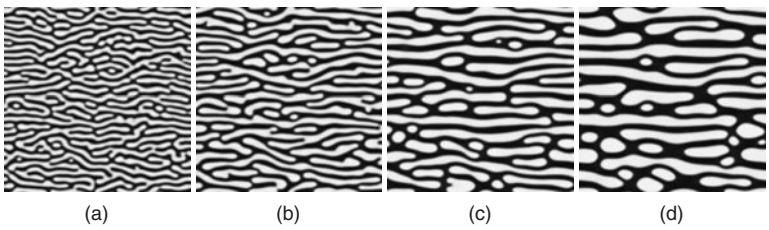

Figure 7. Morphological patterns of coarsening in an elastically isotropic and inhomogeneous system ($K_A = K_B$, $\mu_A = 2\mu_B$) with externally applied strain along the [10] direction ($\epsilon^{\mathrm{a}}_{11} = 0.02$). (a) $t = 40$; (b) $t = 120$; (c) $t = 400$; (d) $t = 1000$.

effect on the morphology. Therefore, there is no driving force for rafting under external stress in the elastic regime if the matrix and precipitate have the same elastic constants [47]. However, for an elastically inhomogeneous system, an externally applied load can dramatically influence the morphological pattern evolutions if the elastic inhomogeneity is significant. Directional coarsening often occurs under applied stress which results in a strong anisotropy of the microstructure. The direction of rafts is dependent on several factors including the sign of the applied strain ϵ^{a}, the sign of the elastic lattice misfit ϵ_0 and the sign of the elastic inhomogeneity θ. The sign of the elastic inhomogeneity θ is defined as positive if elastic moduli increase with the local composition. We define a parameter $S \equiv \theta\epsilon_0\epsilon^{\mathrm{a}}$. It is predicted that if $S > 0$, the orientation of rafts is parallel to the stress axis (type P) [47]. In contrast, if $S < 0$, rafts are formed normal to the stress axis (type N).

Figure 7 shows the microstructures at four different times for an elastically isotropic system with a tensile strain $\epsilon^{\mathrm{a}}_{11} = 0.02$ applied. The shear modulus of the two phases differs from 100% ($\mu_A = 2\mu_B$). Both θ and ϵ_0 are positive ($\epsilon_0 = 0.07$); thus $S > 0$. The hard phase formed the precipitates which were stretched in the direction of the applied strain [10]. Driven by the reduction of the total interfacial energy and elastic energy, the long stripe-shaped precipitates grow at the expense of the shrinkage or dissolution of the small elliptically shaped particles. However, coarsening in an elastically anisotropic system under an applied strain develops different morphologies. An example is shown in figure 8 for a system where the phases have the anisotropy $\xi_{\mathrm{a}} = -1$ and the elastic inhomogeneity θ is 200%. Initially both phases are interconnected and stretched along the [10] direction, forming a lamellar pattern. During microstructure coarsening, the disappearance of bottlenecks between two phases such as D and E in figure 8(c) takes place. The bottlenecks are unstable because of the high stresses around them due to the elastic inhomogeneity. Therefore microstructure will evolve in such a way as to eliminate those bottlenecks. At later stages the morphology forms a parallel alignment of both phases.

Changing the sign of any one of the three, ϵ^{a}, θ and ϵ_0, will change the rafting direction with respect to the axis of the applied load. By using the system in figure 8(d) as the reference, the corresponding morphologies of reversing the signs at $t = 1000$ are shown in figures 9(a)–(c), respectively. Figure 9(a) is the morphology when a compressive strain $\epsilon^{\mathrm{a}}_{11} = -0.02$ is applied to the same system as in figure 8 with all other conditions the same. Figure 9(b) shows the microstructure at the same time step if we only reverse the sign of the composition expansion coefficient, i.e. $\epsilon_0 = -0.07$. It is interesting to note that figures 9(a) and 9(b) are exactly the same. In figure 9(c) the sign of θ is reversed ($\theta < 0$). In this case, phase A, which has a higher equilibrium composition value than phase B, is actually a soft phase. If we change the signs of two of the three parameters, ϵ^{a}, θ and ϵ_0, the precipitates again will align parallel to the axis of applied stress, since the sign of the parameter S is positive. As shown in figure 9(d), the morphology where the signs of both ϵ^{a} and ϵ_0 are reversed is exactly the same

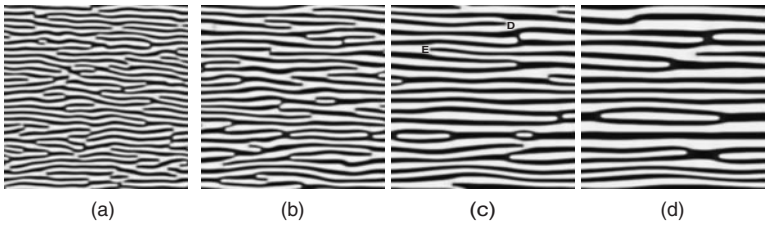

Figure 8. Morphological patterns of coarsening in an elastically anisotropic and inhomogeneous system ($C_{ij}^{A} = 2C_{ij}^{B}$) with externally applied strain along the [10] direction ($\epsilon_{11}^{\mathrm{a}} = 0.02$). (a) $t = 40$; (b) $t = 120$; (c) $t = 400$; (d) $t = 1000$.

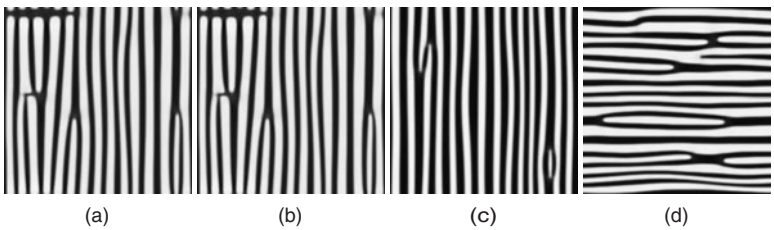

Figure 9. Morphological patterns of coarsening in an elastically anisotropic and inhomogeneous system with externally applied strain along the [10] direction at $t = 1000$ where the signs of the parameters ϵ^{a}, ϵ_0 and θ are reversed. Figure 8(d) is the reference microstructure. (a) Compressive strain $\epsilon_{11}^{\mathrm{a}} = -0.02$ ($S < 0$). (b) Negative composition expansion coefficient $\epsilon_0 = -0.07$ ($S < 0$). (c) Negative elastic inhomogeneity $\theta = -100\%$ ($S < 0$). (d) Compressive strain $\epsilon_{11}^{\mathrm{a}} = -0.02$ and negative composition expansion coefficient $\epsilon_0 = -0.07$ ($S > 0$).

as shown in figure 8(d). If a shear strain $\epsilon_{11}^{\mathrm{a}}$ is applied, we find that the precipitates will then align along the [11] direction.

5. Conclusions

An efficient numerical approach coupling the conjugate gradient method and the Fourier-spectral method has been developed to solve the two-dimensional inhomogeneous elasticity equation and the Cahn–Hilliard equation, which allows very large elastic inhomogeneity. The characteristics of a particular microstructure depend on the elastic properties such as the elastic anisotropy, elastic inhomogeneity and externally applied strain. We have studied the morphological evolution of coarsening for both elastically isotropic and anisotropic systems. It is generally found that the hard phase tends to form precipitates surrounded by the soft matrix phase to reduce the elastic energy, in agreement with prior studies using first-order approximations. It is shown that particle coalescence and splitting may take place simultaneously during coarsening. The growth exponent decreases with increasing elastic inhomogeneity, indicating the slowing down of the coarsening. However, no coarsening freezing is observed, contrary to some previous predictions using first-order approximations. Finally, the effects of an externally applied strain in the elastic regime on the morphology were studied. In an elastically inhomogeneous system, an applied strain can result in the rafting of microstructures if the elastic inhomogeneity is sufficiently large. The orientation of the rafts depends on the signs of the applied strain, composition expansion coefficient and the elastic inhomogeneity. The proposed approach can be easily extended to the study of a three-dimensional real system. In a forthcoming paper we will report on simulations in a real alloy with strong elastic inhomogeneity in three dimensions.

Acknowledgments

The authors are grateful for the financial support by the National Science Foundation under grant nos DMR 96-33719 and DMS 9721413. The simulations were performed at the San Diego Supercomputer Center.

References

[1] Doi M 1996 *Prog. Mater. Sci.* **40** 79
[2] Fratzl P, Penrose O and Lebowitz J L 1999 *J. Stat. Phys.* **95** 1429
[3] Khachaturyan A G and Shatalov G A 1969 *Sov. Phys.–Solid State* **11** 118
[4] Khachaturyan A G 1983 *Theory of Structural Transformations in Solids* (New York: Wiley)
[5] Chen L Q, Wang Y Z and Khachaturyan A G 1991 *Phil. Mag. Lett.* **64** 241
[6] Chen L Q, Wang Y Z and Khachaturyan A G 1992 *Phil. Mag. Lett.* **65** 15
[7] Wang Y, Chen L Q, and Khachaturyan A G 1993 *Acta Metall. Mater.* **41** 279
[8] Nambu S and Sagala D A 1994 *Phys. Rev.* B **50** 5838
[9] Wang Y Z, Wang H Y, Chen L Q and Khachaturyan A G 1992 *J. Am. Ceram. Soc.* **78** 657
[10] Fan D N and Chen L Q 1995 *J. Am. Ceram. Soc.* **78** 1680
[11] Wang Y and Khachaturyan A G 1997 *Acta Mater.* **45** 759
[12] Hu H L and Chen L Q 1998 *J. Am. Ceram. Soc.* **81** 492
[13] Semenovskaya S and Khachaturyan A G 1998 *J. Appl. Phys* **83** 5125
[14] Li D Y and Chen L Q *Acta Mater.* 1998 **46** 639
[15] Wen Y H, Wang Y and Chen L Q 2000 *Acta Mater.* **47** 4375
[16] Artemev A, Jin Y and Khachaturyan A G 2001 *Acta Mater.* **49** 1165
[17] Li Y L, Hu S Y, Liu Z K and Chen L Q 2001 *Appl. Phys. Lett.* **78** 3878
[18] Abinandanan T A, Johnson W C 1993 *Acta Metall. Mater.* **41** 17
[19] Abinandanan T A, Johnson W C 1993 *Acta Metall. Mater.* **41** 27
[20] Thompson M E, Su C S and Voorhees P W 1994 *Acta Metall. Mater.* **42** 2107
[21] Su C H and Voorhees P W 1996 *Acta Mater.* **44** 1987
[22] Su C H and Voorhees P W 1996 *Acta Mater.* **44** 2001
[23] Thornton K, Akaiwa N and Voorhees P W 2001 *Phys. Rev. Lett.* **86** 1259
[24] Eshelby J D 1961 *Prog. Solid Mech.* **2** 89
[25] Johnson W C and Cahn J W 1984 *Acta. Metall.* **32** 1925
[26] Schmidt I and Gross D 1997 *J. Mech. Phys. Solids* **45** 1521
[27] Schmidt I, Mueller R, and Gross D 1998 *Mech. Mater.* **30** 181
[28] Jou H J, Leo P H and Lowengrub J S 1997 *J. Comput. Phys.* **131** 109
[29] Lee J K 1996 *Metall. Mater. Trans.* A **27** 1449
[30] Lee J K 1998 *Mater. Trans. JIM* **39** 114
[31] Onuki A 1989 *J. Phys. Soc. Japan* **58** 3065
[32] Nishimori H and Onuki A 1990 *Phys. Rev.* B **42** 980
[33] Sagui C, Somoza A M, and Desai R 1994 *Phys. Rev.* E **50** 4865
[34] Koyama T, Miyazaki T and Mebed A E 1995 *Metall. Mater. Trans.* A **26** 2617
[35] Li D Y and Chen L Q 1997 *Scr. Mater.* **37** 1271
[36] Laberge C A, Fratzl P and Lebowitz J L 1997 *Acta Mater.* **45** 3949
[37] Sagui C, Orlikowski D, Somoza A and Roland C 1998 *Phys. Rev.* E **58** 569
[38] Onuki A and Furukawa A 2001 *Phys. Rev. Lett.* **86** 452
[39] Hu S Y and Chen L Q 2001 *Acta. Mater.* **49** 1879
[40] Leo P H, Lowengrub J S and Jou H J 1998 *Acta. Mater.* **46** 2113
[41] Barrett R *et al* 1994 *Templates for the Solution of Linear Systems: Building Blocks for Iterative Methods* (Philadelphia, PA: SIAM)
[42] Cahn J W 1961 *Acta. Metall.* **9** 795
[43] Chen L Q and Shen J 1998 *Comput. Phys. Commun.* **108** 147
[44] Zhu J Z, Chen L Q, Shen J and Tikare V 1999 *Phys. Rev.* E **60** 3564
[45] Nishimori H and Onuki A 1991 *J. Phys. Soc. Japan* **60** 1208
[46] Lifshitz M, and Slyozov V V 1961 *J. Phys. Chem. Solids* **19** 35.
[47] Nabarro F R N 1996 *Metall. Mater. Trans.* A **27** 513